

Memory effect in low-density amorphous silicon under pressureNandini Garg,^{1,*} K. K. Pandey,¹ K. V. Shanavas,¹ C. A. Betty,² and Surinder M. Sharma¹¹*High Pressure and Synchrotron Radiation Physics Division, Bhabha Atomic Research Centre, Mumbai 400085, India*²*Chemistry Division, Bhabha Atomic Research Centre, Mumbai 400085, India*

(Received 29 December 2010; revised manuscript received 19 January 2011; published 15 March 2011)

Our investigations on porous Si (π -Si) show that on increase of pressure it undergoes crystalline phase transitions instead of pressure-induced amorphization, as suggested earlier, and the amorphous phase appears only on release of pressure. This amorphous phase, when subjected to higher pressures, transforms *reversibly* to a higher-coordinated primitive hexagonal phase, showing a kind of memory effect which may be the only example of its kind in the elemental solids. First-principles calculations and thermodynamic arguments help understand these observations.

DOI: [10.1103/PhysRevB.83.115202](https://doi.org/10.1103/PhysRevB.83.115202)

PACS number(s): 64.70.Nd, 61.05.cp, 62.50.-p

I. INTRODUCTION

Due to its immense technological importance, silicon is one of the most widely investigated materials. Even in the context of structural changes under different thermodynamic conditions, its behavior has been extensively studied. In particular, under pressure its structures have been shown to evolve to denser and more highly coordinated forms.¹⁻⁸ For example, in the bulk crystalline form, the initial cubic diamond phase of silicon is known to transform to the β -tin structure at 11 GPa and then to the *Imma* phase at 13 GPa, followed by primitive hexagonal (ph), orthorhombic (*Cmca*), hexagonal close packed (hcp), and face centered cubic (fcc) phases at 16, 38, 42, and 78 GPa, respectively. In contrast, the cubic diamond phase of nanocrystalline Si (~ 50 nm) transforms directly to the primitive hexagonal form at 22 GPa, bypassing the β -tin and *Imma* phases observed in the bulk.⁵ Moreover, this transformation has been claimed associated with a shape change of nanocrystallites. Qualitatively, the nonrealization of intermediate phases has been explained in terms of the increased stability field of the diamond phase.⁵

Experimental studies on nanocrystalline porous silicon (π -Si) suggested that the initial cubic phase transforms to a high-density amorphous (HDA) phase at ~ 14 GPa, which on release of pressure, converts to a low density amorphous (LDA) structure.⁹ These observations were rationalized in terms of pressure induced pseudomelting, implied by the negative Clapeyron slope for Si. It may also be noted that the pressure-induced amorphization (PIA) suggested in Ref. 9 was based primarily on Raman measurements. This, in principle, does not rule out the possibility of a transformation to a phase which may not have a Raman-active mode, such as the primitive hexagonal. Energy-dispersive x-ray diffraction (EDXRD) measurements on the same sample had shown pressure-induced annealing of nanocrystalline regions. Since this would have resulted in an increase of the particle size and reduced surface effects, the high-pressure behavior should have been similar to that of surface-terminated nanoparticles.⁵ Although some of these observations have also been supported by theoretical calculations,^{10,11} the role of pressure on phase transitions in π -Si is still not very clear and needs to be reinvestigated experimentally with rather intense and higher-resolution angle-dispersive x-ray diffraction (ADXRD) experiments.

With this view, we have carried out high-pressure experiments on π -Si using angle-dispersive x-ray diffraction and Raman techniques. In contrast with earlier observed PIA in π -Si,⁹ we have observed that the cubic nano π -Si undergoes a crystalline-crystalline phase transition to the primitive hexagonal¹ phase under high pressure at ~ 20 GPa and the amorphous phase arises only on release of pressure (hereafter referred to as the nanoamorphous phase). This observation is consistent with the transformation seen earlier in the case of surface-terminated nanocrystalline Si.⁵ Interestingly the nanoamorphous phase thus obtained transforms reversibly to the ph phase under further pressure cycles. This reversible amorphous-crystalline transformation may be the only example of its kind in elemental solids. In order to investigate the role of particle size in this reversible behavior we have also carried out high-pressure experiments on bulk amorphous silicon. Our results show that the reversible interconversion also takes place in bulk amorphous Si, provided the pressure release is fast, unlike in the case of nanoamorphous Si. We also present theoretical calculations based on density functional theory and a phenomenological nucleation growth model to explain the experimental observations.

II. EXPERIMENTAL DETAILS

The experimental investigations presented here were carried out on π -Si as well as bulk amorphous Si. π -Si was prepared through electrolytic etching.¹² The average particle size of the diamond-structured nanocrystallites of Si embedded in porous silicon was determined by a phenomenological three-dimensional phonon confinement model,^{13,14} given in detail in the Appendix. For experiments on bulk amorphous Si, 99.9% pure amorphous silicon samples were obtained from BHEL (India) and were characterized by Fourier-transform infrared and Raman spectroscopy. The x-ray structure factor [$S(\mathbf{q})$] of amorphous Si at ambient conditions was found to be consistent with tetrahedral coordination.

For high-pressure experiments the sample was loaded in a ~ 150 μm hole, drilled in a preindented tungsten gasket of a diamond-anvil cell (DAC). X-ray diffraction experiments on π -Si were carried out at BL10XU of Spring8 synchrotron, using an x-ray beam of ~ 30 μm (diameter) and $\lambda = 0.3085$ \AA . A 4:1 methanol-ethanol mixture was used as a

pressure-transmitting medium and pressure was estimated using the ruby fluorescence method. For amorphous Si, in addition to the measurements at SPring8, some of the experiments were also performed at the XRD1 beamline of the Elettra synchrotron. For these experiments a few particles of gold were also loaded in the DAC to determine the pressure in the cell. For Raman measurements, an indigenous confocal optics and supernotch-filter-based micro-Raman system was used. A solid state pumped laser of wavelength 532 nm was used as an excitation source.

III. RESULTS AND DISCUSSION

A. X-ray diffraction and Raman spectroscopy

High-pressure Raman and XRD measurements were carried out on π -Si up to pressures of 31 and 39 GPa, respectively. On increase of pressure, the Raman results, shown in Fig. 1, confirm the vanishing of the Raman-active peak of the cubic phase of π -Si beyond 18 GPa. For example, at 23 GPa essentially a flat background is observed. These results are very similar to the results published earlier.⁹ However, our x-ray diffraction results, given in Fig. 2, show that π -Si does not become amorphous at least up to ~ 39 GPa. Instead it transforms to an eight-coordinated ph phase at ~ 20 GPa. At this pressure the most intense [100] and [101] diffraction peaks of the ph phase are clearly visible. These observations are similar to those of Tolbert *et al.*⁵

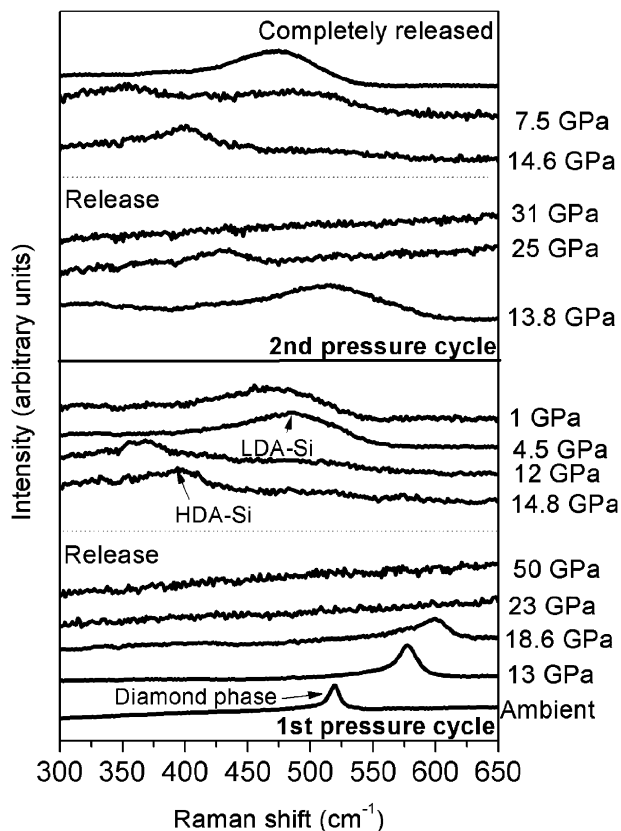


FIG. 1. Raman spectra of π -Si at different pressures. At ambient pressure the Raman peak of the cubic diamond phase can be seen at 519.54 cm^{-1} .

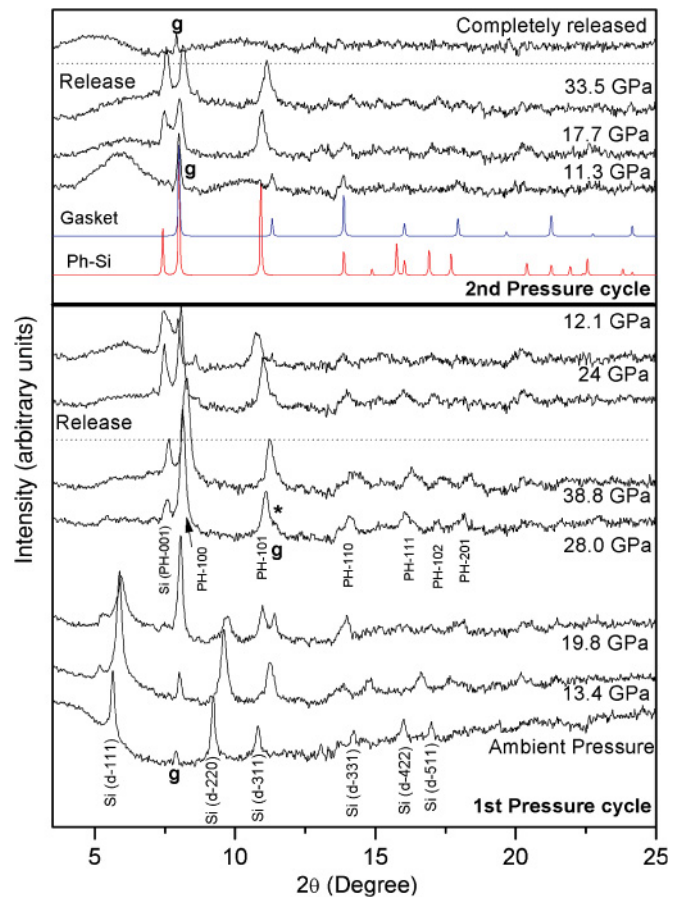


FIG. 2. (Color online) X-ray diffraction patterns of π -Si in the compression and decompression cycles. The background of the empty gasketed cell was subtracted from the diffraction patterns. The pattern at ambient pressure shows all the diffraction peaks of the cubic diamond phase of silicon. The tungsten gasket peaks have been labeled as *g*. The diffraction peaks of the high-pressure phase have been indexed with the ph structure. Calculated diffraction patterns of the ph silicon phase (red) and the gasket peaks (blue) are marked as “gasket” and “Ph-Si.” It can be seen that the diffraction signal at 11.3 GPa in the second pressure cycle is due to the gasket peaks.

The coexistence of the diamond as well as the ph phase of π -Si may be attributed to the first-order nature of the phase transition as well as to the inhomogeneous distribution of local stresses in the sample, aided by pores, etc. In Ref. 9, this crystal-to-crystal phase transition could have been missed due to lack of x-ray diffraction data close to the transition pressure (EDXRD measurements⁹ were carried out up to ~ 15 GPa). Nonobservability of the Raman mode beyond 18 GPa is also misleading as the ph phase does not have any optical phonons and can be easily confused with an amorphous phase. A small difference in the pressure of transformation from that of Tolbert *et al.*⁵ may be understandable in terms of different topology of the nanoparticles. We may also note that in molecular dynamics simulations for bulk Si, the cubic diamond phase has been shown to transform to the ph phase on abrupt pressure increase.¹⁵ It is also known that the β -tin phase becomes inaccessible when Si is compressed at low

temperatures (<100 K).¹⁶ These facts suggest that in its field of stability, even though the β -tin phase is a lower-energy state (as compared to the ph phase), there exists a low-barrier path between the cubic diamond and ph phases. In static high-pressure experiments on bulk Si under ambient temperature, the β -tin phase is realized because there is sufficient relaxation time and thermal energy to overcome the barrier. In the case of nanoparticles, because of the absence of intrinsic defects and the substantial energy contribution due to surface modification (resulting from structural changes), high-barrier paths become inaccessible. Our experimental observation is also supported by the first-principles calculations (described later in this paper) which show instability of the β -tin phase in nanoclusters of Si.

Our Raman results (Fig. 1) do not show the presence of a high-density amorphous phase on subjecting the cubic diamond phase of porous silicon to higher pressures, unlike the results of earlier studies.⁹ It is worth noting that if there is a significant amorphous content in the free-standing porous silicon samples^{17–19} then the signatures of a high-density amorphous phase in the Raman spectrum at high pressures can be mistaken as due to amorphization of cubic diamond silicon.⁹ However, we observed that the ph phase transformed to the HDA phase on release of pressure. The broad band centered at 392 cm^{-1} at ~ 15 GPa, can be assigned to the HDA phase. On further release of pressure the low-density amorphous phase was identifiable at ~ 4.5 GPa, characterized by a broad hump of tetrahedral Si-Si stretching vibrations at 484 cm^{-1} . When this LDA phase was repressurized, it transformed back to the ph phase at ~ 18 GPa, implying a reversible amorphous-to-crystalline phase transformation under pressure. From Fig. 1 it is evident that even in the second pressure cycle the LDA-ph and reverse transformation proceed through a HDA phase. In fact when pressure was released in the second pressure cycle, coexistence of the LDA and HDA phases was observed at ~ 7.5 GPa. Interestingly, the LDA phase obtained on release of pressure remains stable over a prolonged period of time, suggesting that this amorphous phase is either a kinetically preferred state²⁰ or an energetically preferred state in the case of nanoparticles.

Our x-ray diffraction results are also in agreement with the Raman measurements. On release of pressure the XRD pattern shows a small fraction of the amorphous phase at 12 GPa. On further release of pressure to ~ 1 GPa all the diffraction peaks disappear, indicating complete amorphization. This is evident in the second-pressure-cycle diffraction data on the same sample at 11 GPa as shown in Fig. 2, where only gasket peaks are observable other than broad humps due to amorphous Si. The large contribution of gasket peaks at this pressure is due to the fact that the DAC was intentionally moved so that the x-ray beam falls close to the gasket hole edge. It was done to determine whether x rays are bathing the sample completely or not. The DAC was again moved back to the centered position in subsequent pressure runs in order to minimize the gasket contribution. This is also clear from the drastic reduction of the (200) gasket peak intensity at ~ 18 GPa (Fig. 2). At this pressure several new diffraction peaks could be observed, which correspond to the ph-Si phase. The sample completely amorphized on full release of pressure even after the second pressure cycle (Fig. 2). Unfortunately, due to the

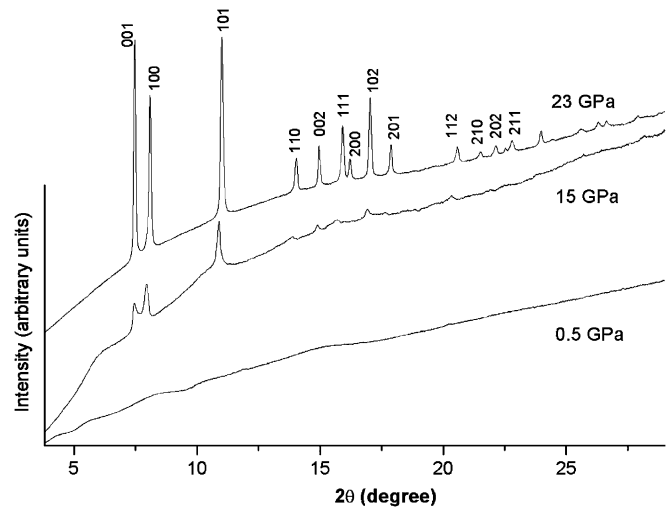


FIG. 3. High-pressure diffraction pattern of amorphous silicon collected at BL-10XU, Spring8. The diffraction peaks in the high-pressure phase have been indexed to the ph phase.

lack of sufficient Q range and the very large background, HDA and LDA phases could not be convincingly identified in XRD measurements. However, both XRD and Raman results confirm the pressure-induced reversible transition between the amorphous and ph phases in π -Si. Here we would like to mention that no elemental solid to our knowledge has been shown to display this kind of memory effect between a crystalline and an amorphous phase.

In order to investigate whether this reversible amorphous-crystal transition exists only in nanoamorphous Si or occurs in general for size-independent amorphous Si *per se*, we carried out high-pressure experiments on the bulk amorphous system also. When the bulk amorphous Si is subjected to high pressure, it also transforms to the primitive hexagonal phase, similar to nanoamorphous Si (Fig. 3). However, in this case the crystallization takes place at a lower pressure of ~ 15 GPa.

Interestingly, the bulk amorphous phase exhibits significant deviation during the decompression process: if the pressure is reduced slowly, it follows the same sequence of transformations as the bulk crystalline Si, i.e., appearance of the β -Sn phase and subsequently the R -8 phase on full release. If decompressed fast enough ($< \sim 60$ s) we get the amorphous (LDA) phase. Repressurizing this LDA again takes it back to the ph phase following the same transformation sequence, i.e., LDA-HDA-ph. To further test whether this sequence of phase transitions depends upon the way the LDA is obtained, we prepared another amorphous (LDA) Si sample from bulk crystalline Si following the pressure-temperature cycle suggested by Imai *et al.*¹⁶ (with the β -Sn phase as a precursor to LDA Si). Our experiments confirm the same reversible nature of the amorphous-ph-amorphous phase transition. Pressure-induced crystallization in amorphous Si has also been observed in a few earlier studies.^{8,21} However, due to more interesting phenomena under consideration, such as the density-driven polyamorphic transition between semiconducting and metallic forms, partial crystallization as indicated by emerging diffraction peaks was overlooked. As

TABLE I. The comparison of the ratios of the calculated d spacings of β -tin and ph phases with those of the experimental results of Ref. 21.

Data from calculated pattern of β -tin		Data from calculated pattern of ph		Data read from Fig. 3 of Ref. 21	
hkl	d ratio	hkl	d ratio	hkl as indexed in Ref. 5 to β -tin	d ratio
(200)/(220)	1.414 90	(100)/(101)	1.3648	(200)/(220)	1.485
		(001)/(101)	1.47	(220)/(301)	1.272
(220)/(301)	1.2407	(101)/(110)	1.2685	(220)/(400)	1.4692
(220)/(400)	1.4142	(101)/(111)	1.44	(220)/(420)	1.653 ¹
(220)/(420)	1.581 01	(101)/(102)	1.544		

¹This ratio is not very accurate as the diffraction peak (420) of Fig. 3 is very weak and broad.

these peaks appear in the stability regime of the metallic β -Sn phase with a coordination number similar to that of the HDA phase, those studies interpreted the high-pressure phase to be the β -Sn phase.^{8,21} To ensure the correctness of our inference, we have calculated the diffraction patterns of both ph and β -tin phases of silicon and compared the different ratios of d values with those of the observed diffraction pattern of Ref. 21. As shown in Table I, the ratios of the d values of the ph phase are closer to the experimentally observed values. Therefore the ph phase is a more appropriate representation for the high-pressure phase.

B. Theoretical calculations

The crystalline phase transition as observed in the first pressure cycle of porous silicon from the cubic diamond to the ph phase could have occurred due to a homogeneous deformation mechanism. However, the crystallization observed in subsequent pressure cycles in porous silicon, i.e., from the amorphous to the preferred ph phase, can be understood in terms of thermodynamic arguments used earlier by others²² to explain the pressure-induced crystallization of glass. The crystallization of an amorphous phase is known to be a nucleation and growth process which involves formation of a low-density interface layer between the crystalline nucleus and amorphous matrix. During homogeneous nucleation, the change in Gibbs free energy due to formation of a spherical crystalline nucleus of diameter d in an amorphous matrix is given as

$$\Delta G^n(T, P) = \frac{(1/6)\pi d^3}{V^c}(\Delta G^{am \rightarrow c}) + \pi d^2 \sigma + P \Delta V, \quad (1)$$

where $\Delta G^{am \rightarrow c}$ is the molar free energy change for the transformation from the amorphous to the crystalline phase, σ is the interfacial energy per unit area, V^c is the molar volume of the crystalline phase, and ΔV is the volume change during the formation of the crystalline nucleus.²² The net volume change due to nucleation depends on the size of the nucleus and the molar volumes of crystalline and amorphous phases and the interface layer. The thermodynamic barrier for nucleation, i.e., nucleation work ΔG^* , and the critical diameter d^* of the nucleus can be determined from the condition $\partial \Delta G^n / \partial d = 0$. This gives

$$\Delta G^* = \frac{16\pi\sigma^3}{3(\Delta G^{am \rightarrow c} / V^c)^2}.$$

We have estimated $\Delta G^{am \rightarrow c}$ from the enthalpies of the crystalline and amorphous phases at 0 K. The interfacial energy has been taken to be 0.49 J/m².²³ These calculations show that although the thermodynamic barrier ΔG^* for the crystallization of both ph and β -tin decreases with increasing pressure, at ~ 15 GPa the thermodynamic barrier for crystallization of the ph phase is $\sim 20\%$ lower than that of the β -tin phase. This suggests that since the nucleation work required for growth of critical nuclei of β -tin phase is higher at this pressure, there will be a preferential crystallization to the ph phase. Further, under high pressures, the pressure derivative of the volume is always negative in congruence with the second law of thermodynamics. Therefore, the crystallization becomes feasible only when thermodynamic state of the system allows formation of nuclei of sizes greater than the critical value, for which the net volume change is zero or negative. Using the equation of state (EOS) of crystalline and amorphous phases and the interfacial energy, we can estimate the volume change as a function of nucleus size for each pressure and hence the pressure of crystallization. Using the EOSs for the cubic, β -Sn, ph, LDA and HDA phases of silicon, obtained from density functional theory (DFT) calculations,^{24–26} we have estimated the crystallization pressures of various crystalline phases, shown in Table II. Of course this assumes that no other physical process restrains the crystallization.

From this table we can see that the crystallization pressure of the cubic phase lies beyond its stability region and hence it cannot be realized. Our calculations show that crystallization of β -Sn and ph phases from the HDA phase could be feasible at ~ 12 and ~ 18 GPa, respectively (provided the HDA phase exists at these pressures). However, with the help of first-principles calculations Durandurdu *et al.*²⁶ have shown that the HDA phase of silicon is formed only above 15 GPa (which is well above the crystallization pressure of β -Sn determined from our calculations). Based on these calculations

TABLE II. The crystallization pressures of transition of low-density and high-density amorphous silicon to different crystalline phases, determined from thermodynamic modeling.

Amorphous phase	Crystalline phase	Pressure of crystallization
LDA	Diamond	19 GPa
HDA	β -Sn	12 GPa
HDA	ph	18 GPa

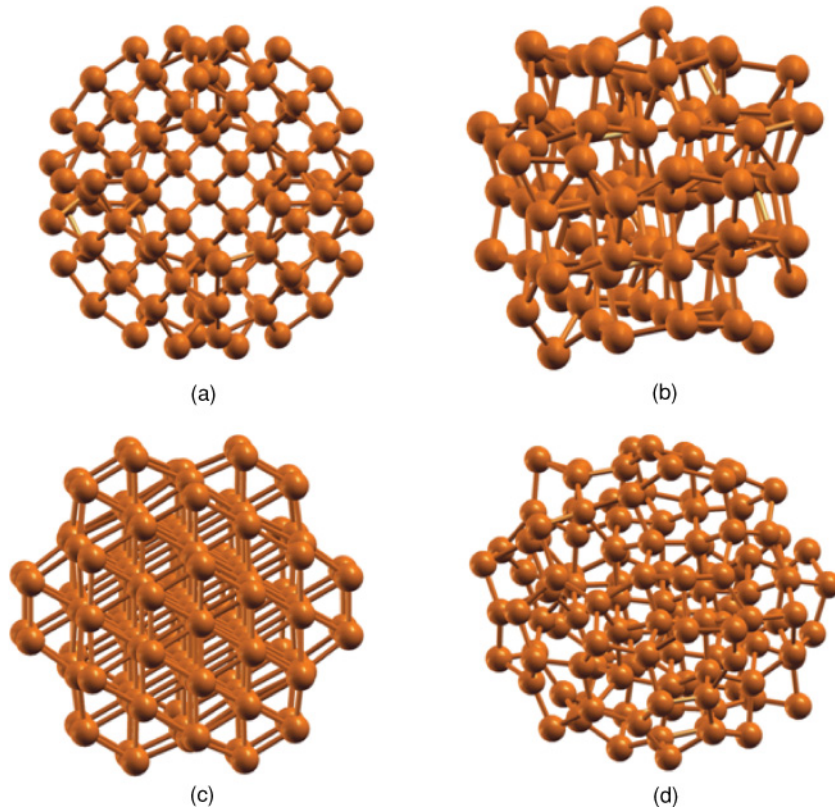


FIG. 4. (Color online) Clusters of different structures of silicon as simulated by first-principles calculations. (a) The diamond cluster has the lowest energy among the stable crystal clusters. (b) β -tin becomes disordered upon relaxation but retains somewhat higher coordination. (c) Primitive hexagonal phase forms a more compact cluster although with a higher energy. (d) The amorphous structure has almost the same volume as the diamond structure but has the lowest energy.

we conclude that the HDA phase of silicon preferentially crystallizes to the ph phase.²⁷

To gain further insights, particularly in the context of transformation of the ph phase (obtained from π -Si) to the LDA phase on release of pressure, several first-principles calculations were carried out on Si nanoclusters. DFT calculations were used to optimize the ionic positions of small silicon clusters of approximately ~ 110 atoms and diameter ~ 1.4 nm. Structural relaxations were performed within the

generalized gradient approximation²⁸ using the projector augmented wave²⁹ method as implemented in the Vienna *ab initio* simulation package³⁰ (VASP) starting from spherical clusters. An energy cutoff of 400 eV with Γ point sampling was used to find the lowest-energy configurations of clusters in a 20 Å supercell. The amorphous structure was generated by heating a cubic silicon cluster to 1500 K and quenching it. Molecular dynamics simulations were then carried out for 0.3 ps at 300 K to equilibrate the cluster which was then subsequently optimized at 0 K. The resultant cluster had almost the same volume as the diamond structure.

The structures of the different phases of silicon, obtained after structural optimization, are shown in Fig. 4. Our results indicate that for these small clusters, the amorphous phase has lower energy than even the cubic diamond structure (difference in energy/atom of 67.9 meV). We found that the β -tin structure does not stabilize in small clusters whereas diamond and simple hexagonal structures are retained under structural optimization. These calculations suggest that in the case of nanoclusters, the cubic diamond phase is actually a metastable state as compared to the relatively more stable LDA phase and hence emergence of this phase on release of pressure is basically kinetics independent. These calculations also explain the nonobservability of the β -tin phase in π -Si. A similar size-dependent structural transformation has been observed recently in silver.³¹

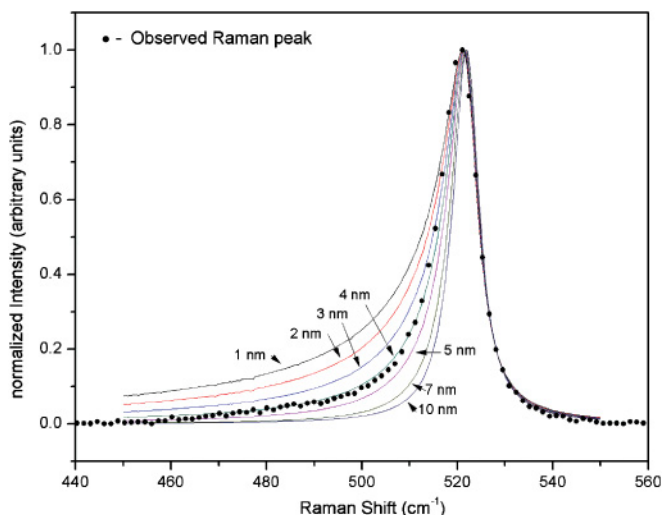


FIG. 5. (Color online) Observed first-order Raman peak of π -Si (dotted profile). Calculated Raman peak profile for different average particle sizes (solid lines). The calculated profile of the 4-nm-sized particle shows the best fit to the experimental Raman spectra of π -Si.

IV. CONCLUSIONS

In conclusion, we have observed a pressure-induced reversible amorphous-crystalline transformation in an elemental solid; which should encourage further experimental as well as

theoretical studies. π -Si does not amorphize on compression and instead it undergoes a crystalline transformation and the amorphous phase arises only on decompression. Moreover, our studies show that irrespective of the method of preparation or size of the amorphous Si particles, it always transforms to the primitive hexagonal phase under compression.

APPENDIX

For nanocrystals, momentum conservation is no longer valid since the optical phonons are localized. This allows optical phonons of $q \neq 0$ to contribute to the Raman scattering. Therefore the first-order Raman intensity $I'(\omega, L)$ for quantum-dot-like structures having three-dimensional confinement is given by

$$I'(\omega, L) \propto \int_0^1 \frac{\exp(-q^2 L^2 / 4a^2)}{\{[\omega - \omega(q)]^2 + (\Gamma/2)^2\}} d^2 q, \quad (\text{A1})$$

where $\omega(q)$ represents the phonon dispersion curve for the optical branch of c -Si and a is the lattice constant. Γ is the natural linewidth and L is the quantum confinement diameter. The dispersion relation was taken to be $\omega(q) = \omega(1 - 0.18q^2)$ which fits the experimental dispersion curve.³² The Raman frequency ω and lattice constant a were taken to be 520 cm^{-1} and 5.43 \AA , respectively. Assuming a Gaussian distribution of particle size given by $N(L) \cong \{\exp[-(L - L_0)^2 / 2\sigma^2]\}$, the final intensity of first-order Raman scattering was calculated using following equation:

$$I(\omega) \propto \int_{L_1}^{L_2} N(L) I'(\omega, L) dL \quad (\text{A2})$$

σ is the standard deviation and L_0 is the mean particle size. As shown in Fig. 5, the best fit for the observed Raman peak was obtained for average particle size $L_0 = 4 \text{ nm}$ with standard deviation $\sigma = 2 \text{ nm}$.

*Corresponding author: nandini@barc.gov.in

¹H. Olijnyk, S. K. Sikka, and W. B. Holzapfel, *Phys. Lett. A* **103**, 137 (1984).

²P. F. McMillan, M. Wilson, M. C. Wilding, D. Daisenberger, M. Mezouar, and G. N. Greaves, *J. Phys.: Condens. Matter* **19**, 415101 (2007).

³J. C. Jamieson, *Science* **139**, 762 (1963).

⁴R. H. Wentorf and J. H. Kasper, *Science* **139**, 338 (1963).

⁵S. H. Tolbert, A. B. Herhold, L. E. Brus, and A. P. Alivisatos, *Phys. Rev. Lett.* **76**, 4384 (1996).

⁶S. H. Tolbert and A. P. Alivisatos, *Annu. Rev. Phys. Chem.* **46**, 595 (1995).

⁷H. K. Poswal, N. Garg, S. M. Sharma, E. Busetto, S. K. Sikka, G. Gundiah, F. L. Deepak, and C. N. R. Rao, *T. Nanosci. Nanotech.* **5**, 729 (2005).

⁸V. Domnich and Y. Gogotsi, *Rev. Adv. Mater. Sci.* **3**, 1 (2002).

⁹S. K. Deb, M. C. Wilding, M. Somayazulu, and P. F. McMillan, *Nature (London)* **414**, 528 (2001).

¹⁰M. Durandurdu and D. A. Drabold, *Phys. Rev. B* **66**, 205204 (2002).

¹¹R. Martoňák, C. Molteni, and M. Parrinello, *Phys. Rev. Lett.* **84**, 682 (2000).

¹²Y. H. Xie, M. S. Hybertsen, W. L. Wilson, S. A. Ipri, G. E. Carver, W. L. Brown, E. Dons, B. E. Weir, A. R. Kortan, G. P. Watson, and A. J. Liddle, *Phys. Rev. B* **49**, 5386 (1994).

¹³H. Richter, Z. P. Wang, and L. Ley, *Solid State Commun.* **39**, 625 (1981).

¹⁴I. H. Campbell and P. M. Fauchet, *Solid State Commun.* **58**, 739 (1986).

¹⁵P. Focher, G. L. Chiarotti, M. Bernasconi, E. Tosatti, and M. Parrinello, *Europhys. Lett.* **26**, 345 (1994).

¹⁶M. Imai, T. Mitamura, K. Yaoita, and K. Tsuji, *High Press. Res.* **15**, 167 (1996).

¹⁷R. Tsu, H. Shen, and M. Dutta, *Appl. Phys. Lett.* **60**, 112 (1992).

¹⁸Z. Sui, P. P. Leong, I. P. Herman, G. S. Higashi, and H. Temkin, *Appl. Phys. Lett.* **60**, 2086 (1992).

¹⁹S. K. Deb, In *Advances in High Pressure Science and Technology*, Proceedings of the Fourth NCHST, IGCAR, Kalpakkam, India, edited by M. Yousuf, N. Subramian, and R. K. Govind (Universities Press, India, Hyderabad, 1997), pp. 147–152.

²⁰S. M. Sharma and S. K. Sikka, *Progr. Mater. Sci.* **40**, 1 (1996).

²¹D. Daisenberger, M. Wilson, P. F. McMillan, R. Q. Cabrera, M. C. Wilding, and D. Machon, *Phys. Rev. B* **75**, 224118 (2007).

²²F. Ye and K. Lu, *Phys. Rev. B* **60**, 7018 (1999).

²³N. Bernstein and M. J. Aziz, and E. Kaxiras, *Phys. Rev. B* **58**, 4579 (1998).

²⁴K. K. Pandey, N. Garg, K. V. Shanavas, S. M. Sharma, S. K. Sikka (unpublished). The details of these calculations, which deduce the crystallization in terms of the critical size of nuclei under pressure, will be presented elsewhere.

²⁵K. V. Shanavas, K. K. Pandey, N. Garg, S. M. Sharma (unpublished). The computer simulation of crystallization kinetics in amorphous silicon under pressure will be presented elsewhere.

²⁶M. Durandurdu and D. A. Drabold, *Phys. Rev. B* **64**, 014101 (2001).

²⁷For consistency all the parameters of the model have been taken from the first-principles calculations (i.e., Refs. 13 and 31).

²⁸J. P. Perdew, K. Burke, and M. Ernzerhof, *Phys. Rev. Lett.* **77**, 3865 (1996); J. P. Perdew, K. Burke, and Y. Wang, *Phys. Rev. B* **54**, 16533 (1996).

²⁹P. E. Blöchl, *Phys. Rev. B* **50**, 17953 (1994).

³⁰G. Kresse and J. Hafner, *Phys. Rev. B* **47**, R558 (1993); G. Kresse and J. Furthmüller, *ibid.* **54**, 11169 (1996).

³¹J. Fang, H. You, P. Kong, B. Ding, and X. Songa, *Appl. Phys. Lett.* **92**, 143111 (2008).

³²W. Weber, *Phys. Rev. B* **15**, 4789 (1977).